Phase-matched rectangular magnetooptic waveguides for applications in integrated optics isolators: Numerical assessment

M. Lohmeyer, N. Bahlmann, O. Zhuromskyy, H. Dötsch, P. Hertel*
Department of Physics, University of Osnabrück,
Barbarastraße 7, D-49069 Osnabrück, Germany

Abstract: Phase matching between the fundamental TE and TM modes is an essential condition for complete polarization rotation in magnetooptic waveguides with longitudinally directed magnetization. This condition can be satisfied with embedded square waveguides or with raised strip waveguides, provided that the core dimensions are suitably chosen. Based on coupled mode theory for the vectorial modes of rectangular isotropic waveguides, we numerically simulate the performance of such devices in an experimental isolator setup, including birefringence and optical absorption. Fabrication tolerances with respect to all relevant parameters can be evaluated by simple perturbational expressions. Numerical verification shows that these formulas are accurate enough for practical purposes. The tolerances qualify the traditional polarization rotator setup as competitive to recent proposals for integrated optical isolators based on nonreciprocal interferometry.

Keywords: integrated optics, magnetooptic waveguides, numerical modeling, Faraday effect, optical isolators, fabrication tolerances
PACS codes: 42.82.–m 42.82.Et 85.70.Sq 78.20.Ls

1 Introduction

Besides a series of proposals exploiting the nonreciprocal phase shift in magnetooptic waveguides, most theoretical and experimental work on integrated optical isolators was concerned with setups analogous to microoptic devices where the waveguide is used as a nonreciprocal polarization rotator between two polarizers. One of the major problems with this concept in integrated form is to overcome form birefringence: usually the propagation constants for modes of different polarizations are different. This limits the maximum power transfer ratio and thus deteriorates the isolation. To achieve phase-matching for TE- and TM-like modes, a number of techniques were proposed. Among these are the periodic reversal of the magnetization [1], the use of anisotropic top layers [2], of multilayered waveguide structures [3], growth induced birefringence [4], the application of stress [5], Dammann's geometry [6], and thickness tuning for planar [7] and ridged waveguides [8].

In contrast to planar waveguides, for rib waveguides there are certain configurations where the wavenumbers for modes of both dominant polarizations are exactly equal. This can be realized as follows. For a planar-like raised strip waveguide with a thin and wide core, usually the propagation constant of the fundamental TE mode exceeds that of the fundamental TM mode. If the rib is continuously narrowed and raised, the device becomes a planar-like waveguide again, but with the role of the transverse axes exchanged. Consequently there is an intermediate configuration with almost square core and phase matched modes. This paper gives a detailed numerical analysis of the effects relevant for isolating performance with emphasis on fabrication tolerances.

The coupled mode theory as formulated in the following section is based on vectorial modes of isotropic lossless cores, with the linear magnetooptic effect, linear birefringence, and isotropic absorption considered as perturbations. Sec. 3 fixes a model for an isolator setup. In Sec. 4, first order expansions of the degree of polarization conversion lead to simple perturbational expressions for fabrication tolerances of all structural parameters. These formulas are applied to a series of raised strip waveguides and compared to directly numerically evaluated tolerances in the main part of Sec. 5.

Obviously a direct way to achieve phase matching is to use a square core embedded in a homogeneous cladding. Sec. 5.2 reports on our results for such waveguides.

* *Fachbereich Physik, Universität Osnabrück* *Barbarastraße 7, D 49069 Osnabrück*
Tel.: +541/969-2641 *Fax: +541/969-2670* *e-mail: manfred.lohmeyer@physik.uni-osnabrueck.de*

2 Vectorial coupled mode theory

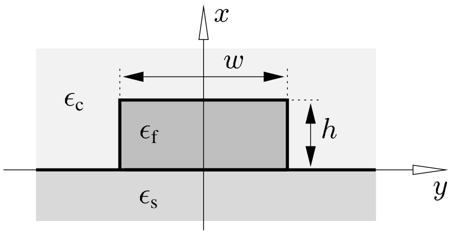

Figure 1: A simple raised strip waveguide. Structural parameters are the height h and width w of the rib and the permittivities ϵ_s, ϵ_f, ϵ_c of the substrate, the guiding film, and the cover material, respectively. x and y denote the cross section coordinate axes, with the y-direction parallel to the substrate surface. Light propagates along the z-axis.

Fig. 1 sketches the rectangular waveguides with piecewise constant permittivity investigated in this paper. We assume the substrate and cover layers to be made of lossless isotropic material with homogeneous permittivities $\epsilon_s = n_s^2$ and $\epsilon_c = n_c^2$. The permittivity tensor for the magnetooptic core region $\epsilon_f = n_f^2 + \Delta\epsilon$ is split into the contribution of an isotropic lossless refractive index n_f and a residual $\Delta\epsilon$, a perturbation. $\Delta\epsilon$ is again a sum of several terms which are specified in Sec. 2.1 – 2.3. Without them, the guided electric and magnetic fields $\boldsymbol{\mathcal{E}}$ and $\boldsymbol{\mathcal{H}}$ are superpositions

$$\boldsymbol{\mathcal{E}}(x,y,z,t) = \sum_j C_j(z)\,\frac{1}{\sqrt{P_j}}\boldsymbol{E}_j(x,y)\exp(\mathrm{i}\omega t), \quad \boldsymbol{\mathcal{H}}(x,y,z,t) = \sum_j C_j(z)\,\frac{1}{\sqrt{P_j}}\boldsymbol{H}_j(x,y)\exp(\mathrm{i}\omega t) \qquad (1)$$

of the hybrid mode fields $\boldsymbol{E}_j$, $\boldsymbol{H}_j$ with coefficients $C_j(z) = C_{j0}\exp(-\mathrm{i}\beta_j z)$ that include the harmonic dependence on the propagation distance. P_j is the power assigned to mode j. The β_j denote the propagation constants at a frequency ω corresponding to the vacuum wavelength λ and wavenumber $k = 2\pi/\lambda = \omega\sqrt{\epsilon_0\mu_0}$, for vacuum permittivity ϵ_0 and permeability μ_0.

The unperturbed mode fields are of the form $\boldsymbol{E}_j = (E_{jx}, E_{jy}, \mathrm{i}E_{jz})$, $\boldsymbol{H}_j = (H_{jx}, H_{jy}, \mathrm{i}H_{jz})$, with real valued components. Due to the symmetry of the guiding profile with respect to the reflection $y \to -y$, the components have a definite parity. In this paper, we call a mode with even components H_{jx}, E_{jy}, H_{jz} and odd components E_{jx}, H_{jy}, E_{jz} symmetric, one with reversed symmetry antisymmetric. For modes propagating in the same direction the orthogonality property

$$\frac{1}{2}\iint (E_{jx}H_{ky} - E_{jy}H_{kx})\,\mathrm{d}x\,\mathrm{d}y = \delta_{jk}P_j \qquad (2)$$

holds, with $\delta_{jk} = 1$ for $j = k$, $\delta_{jk} = 0$ otherwise.

Assuming that the guided field in the waveguide with the full permittivity ϵ_f can be expanded into the unperturbed guided modes as well, the superposition (1) remains valid, but the amplitudes are no longer of simple harmonic dependence on z. With the help of Maxwell's equations, the following reciprocity identity can be derived straightforwardly [9]:

$$\mathrm{div}(\boldsymbol{\mathcal{H}} \times \boldsymbol{\mathcal{E}}_j^* - \boldsymbol{\mathcal{E}} \times \boldsymbol{\mathcal{H}}_j^*) = \mathrm{i}\omega\epsilon_0 \boldsymbol{\mathcal{E}}_j^*\,\Delta\epsilon\boldsymbol{\mathcal{E}}\,. \qquad (3)$$

Here $\boldsymbol{\mathcal{E}}_j$, $\boldsymbol{\mathcal{H}}_j$ denote the mode fields with additional time and space dependence $\sim \exp(\mathrm{i}\omega t - \mathrm{i}\beta_j z)$. Integration over the x-y-plane, insertion of (1), and use of (2) yields equations for the coupled mode amplitudes

$$\partial_z C_j = -\mathrm{i}\beta_j C_j - \mathrm{i}\sum_k \kappa_{jk} C_k, \qquad (4)$$

where the coupling coefficients κ_{jk} are given by

$$\kappa_{jk} = \frac{\omega\epsilon_0}{4\sqrt{P_j P_k}} \iint_\Box \boldsymbol{E}_j^*\,\Delta\epsilon\boldsymbol{E}_k\,\mathrm{d}x\,\mathrm{d}y\,. \qquad (5)$$

The box $\Box$ indicates integration over the core region where $\Delta\epsilon$ differs from zero. Note that in general the diagonal coefficients κ_{jj} do not vanish. In fact, Eq. (5) resembles the common perturbational expression for the propagation constant shift due to a permittivity variation, which has been applied frequently e.g. in the simulation of nonreciprocal phase shifters [10, 11, 12]. Thus the coupled mode approach allows to investigate the polarization rotating and phase-shifting effects of an arbitrarily directed magnetization simultaneously.

We now specialize to the case of only the fundamental hybrid symmetric and antisymmetric mode. This is justified if either the waveguide supports these two modes only, or if the initial amplitudes of the remaining ones and their coupling to the fundamental modes is negligible. Both assumptions will be checked numerically for the multimode waveguides in Sec. 5. The E_y component of the fundamental symmetric mode turned out to be much larger than E_x, thus it may be called TE-like, with the TE-direction defined by the substrate surface. The fundamental antisymmetric mode has the roles of E_y and E_x reversed, so its commonly called TM-like. We are interested in relatively high and narrow cores, thus frequently the propagation constant of the TM-like mode exceeds that of the TE mode.

For Hermitian $\Delta\epsilon$ (remarks on lossy core material will follow below), the coupled mode equations reduce to

$$\partial_z C_1 = -\mathrm{i}\beta_1' C_1 - \mathrm{i}\kappa C_2 \,, \qquad \partial_z C_2 = -\mathrm{i}\beta_2' C_2 - \mathrm{i}\kappa^* C_1 \,, \tag{6}$$

with $\beta_j' = \beta_j + \kappa_{jj}$ and $\kappa = \kappa_{12}$. Their solution is

$$\begin{pmatrix} C_1 \\ C_2 \end{pmatrix}(z) = \exp(-\mathrm{i}\frac{\beta_1' + \beta_2'}{2} z) \begin{pmatrix} \cos\rho z - \mathrm{i}\dfrac{\Delta\beta'}{2\rho}\sin\rho z & -\mathrm{i}\dfrac{\kappa}{\rho}\sin\rho z \\ -\mathrm{i}\dfrac{\kappa^*}{\rho}\sin\rho z & \cos\rho z + \mathrm{i}\dfrac{\Delta\beta'}{2\rho}\sin\rho z \end{pmatrix} \begin{pmatrix} C_{10} \\ C_{20} \end{pmatrix} , \tag{7}$$

where ρ is defined as $\rho = \sqrt{(\Delta\beta'/2)^2 + |\kappa|^2}$. Projection on an initial field $(\boldsymbol{E}_{\text{in}}, \boldsymbol{H}_{\text{in}})(x, y)\exp(-\mathrm{i}\omega t)$ gives the amplitudes C_{j0} at $z = 0$:

$$C_{j0} = \frac{1}{2\sqrt{P_j}} \iint (E_{jx} H^*_{\text{in},y} - E_{jy} H^*_{\text{in},x})\,\mathrm{d}x\,\mathrm{d}y \,. \tag{8}$$

The device will be used as a polarization-rotator. Starting at $z = 0$ with all power concentrated in mode 1, after a distance z the relative power $\eta(z) = |C_2(z)/C_{10}|^2$ carried by mode 2 is

$$\eta(z) = \eta_{\text{max}} \sin^2 \rho z \quad \text{with} \quad \eta_{\text{max}} = \frac{|\kappa|^2}{(\Delta\beta'/2)^2 + |\kappa|^2} \,. \tag{9}$$

The power transfer ratio η reaches its maximum η_{max} at the position of the conversion length $L_{\text{c}} = \pi/2\rho$. Note that the mismatch $\Delta\beta' = \beta_1' - \beta_2'$ between the phase-shifted propagation constants determines the upper limit of the polarization conversion.

2.1 Magnetooptic core

The core permittivity contribution $\Delta\epsilon_{\text{mo}}$ due to the linear magnetooptic effect can be written

$$\Delta\epsilon_{\text{mo}} = \mathrm{i}\xi \begin{pmatrix} 0 & \cos\theta & -\sin\theta \\ -\cos\theta & 0 & 0 \\ \sin\theta & 0 & 0 \end{pmatrix} . \tag{10}$$

It represents the effect of a static magnetization adjusted at an angle θ with respect to the z-axis in the y-z-plane parallel to the substrate. ξ is related to the specific Faraday-constant Θ_{F} by $|\xi| = n_{\text{f}}\lambda\Theta_{\text{F}}/\pi$. Symmetry arguments allow to split the coefficients as

$$\kappa^{\text{mo}}_{jj} = \xi \sin\theta \frac{\omega\epsilon_0}{2P_j} \iint_\Box E_{jx} E_{jz}\,\mathrm{d}x\,\mathrm{d}y \tag{11}$$

and

$$\kappa^{\text{mo}}_{jk} = \mathrm{i}\xi \cos\theta \frac{\omega\epsilon_0}{4\sqrt{P_j P_k}} \iint_\Box (E_{jx} E_{ky} - E_{jy} E_{kx})\,\mathrm{d}x\,\mathrm{d}y \quad \text{for} \quad j \neq k \,. \tag{12}$$

(11) is the nonreciprocal phase shift for the TM-like mode. This shift remains small since the integrated product of the E_x- and E_z-fields almost vanishes. For the TE-like mode the phase shift is two orders of magnitude smaller due to its tiny E_x-component. The off-diagonal coupling coefficients $\kappa = \kappa_{12} = \kappa_{21}^*$ (12) drive the mode coupling. They combine only those parts of the fields which are in the core area. Therefore the conversion length in the waveguide exceeds the length $L_c^{\text{bulk}} = n_f \lambda/2\xi = \pi/2\Theta_F$ for plane waves in a bulk medium.

An inclination of the magnetization with respect to the y-z-plane adds a tiny contribution to the coupling coefficient, but it does not lead to a phase shift (which would be proportional to $\iint_\Box E_{jy} E_{jz}\, dx\, dy$), since the coupled E_y- and E_z-fields are of different symmetry. This argument applies to both TE and TM modes, but it is no longer valid for a nonsymmetric structure, e.g. for a waveguide with a vertical domain wall at the center of the rib [12].

Changing the sign of the frequency simulates backward light propagation. Maxwell's equations are satisfied, if for unchanged electric fields and propagation constants the signs of all magnetic fields are reversed. Since ξ is proportional to the static magnetization, its sign must be changed as well. With respect to the polarization rotation, propagation of the backward travelling modes over a negative distance $-z$ becomes equivalent to the propagation of the forward modes over the distance z. At the same time the magnetooptic phase shift is reversed due to $\xi \to -\xi$ (formally in the denominator of Eq. (5) the negative root of $|P_j P_k|$ appears which cancels the negative sign of ω). Thus we can model backward light propagation using Eq. (7) with positive z, with unchanged $\kappa = \kappa_{12}^{\text{mo}}$, but with the signs of κ_{jj}^{mo} reversed.

2.2 Diagonal anisotropy

For a typical YIG-film grown on a (111)-oriented GGG-substrate, growth- and stress-induced anisotropies cause the diagonal component at the x-position of the permittivity tensor to be different from the elements on y- and z-positions [13]. We account for this effect by a dimensionless anisotropy parameter a in the corresponding permittivity perturbation:

$$\Delta\epsilon_{\text{anis}} = \frac{a}{2} \begin{pmatrix} -1 & 0 & 0 \\ 0 & 1 & 0 \\ 0 & 0 & 1 \end{pmatrix} . \tag{13}$$

While $\Delta\epsilon_{\text{anis}}$ does not contribute to the coupling coefficients κ due to the mode symmetry, it is responsible for additional phase shifts

$$\kappa_{jj}^{\text{anis}} = \frac{a}{2} A_j \quad \text{with} \quad A_j = \frac{\omega\epsilon_0}{4P_j} \iint_\Box (-|E_{jx}|^2 + |E_{jy}|^2 + |E_{jz}|^2)\, dx\, dy \, . \tag{14}$$

2.3 Absorption

If the core material attenuates the intensity of a plane wave according to $\sim \exp(-Dz)$ with a small attenuation constant D, this effect can be modeled by an isotropic but imaginary permittivity perturbation $\Delta\epsilon_{\text{abs}} = -\mathrm{i} n_f D/k$. According to Eq. (5), the propagation constants β_j get imaginary parts

$$\kappa_{jj}^{\text{abs}} = -\mathrm{i}\alpha_j/2 \, , \quad \text{with} \quad \alpha_j = D \sqrt{\frac{\epsilon_0}{\mu_0}} \frac{n_f}{2P_j} \iint_\Box |\boldsymbol{E}_j|^2 dx\, dy \, . \tag{15}$$

If we adopt the approximation of equal attenuation for both modes, the propagation equations (7) transfer to the lossy system. Both amplitudes C_j must be multiplied by a factor $\exp(-\alpha z/2)$, where α is the average attenuation $\alpha = (\alpha_1 + \alpha_2)/2$, and the device of length L shows an additional power loss $\sim \exp(-\alpha L)$.

This approximation amounts to neglecting terms $(\alpha_1 - \alpha_2)/4|\kappa|$ and $\sim \Delta\beta'(\alpha_1 - \alpha_2)/|\kappa|^2$. The latter vanish for phase matched waveguides. The former should have an effect comparable to a phase difference $\Delta\beta'/2|\kappa|$. If one can tolerate an error in η up to 10^{-3}, then $(\alpha_1 - \alpha_2)/4|\kappa|$ must not exceed 0.03. This condition is indeed fulfilled, as we will show in Sec. 5.

However, for larger differences in the mode attenuations α_1, α_2, Eqs. (7) have to be modified. This will be necessary for materials with higher losses, if the relevant mode fields differ considerably, or if the damping must be assumed anisotropic. The latter may be the case, if the absorption related to the Faraday rotation (magnetic circular dichroism) turns out to be nonnegligible. Note that the type of damping introduced here models the intrinsic material absorption only.

3 Simulation of an experimental setup

The isolator setup employs a magnetooptic polarization rotating waveguide of total length $L = L_c/2$ which is set between a front polarizer adjusted to the TE-position and a back polarizer at an angle of 45° with respect to the y-direction.

Simulation of forward propagating light starts with a TE-polarized Gaussian beam (input power P_{in}) whose diameter and maximum location has been adjusted to the mode profile average. It passes the front polarizer without modification. Overlap (8) with the mode profiles yields the initial amplitudes for coupled mode propagation along a distance $L = L_c/2$. The output power $P^{\text{f}}_{\text{out}}$ is then determined by projecting $\boldsymbol{\mathcal{E}}$ on a unit vector $\boldsymbol{n} = (\sin\alpha_{\text{o}}, \cos\alpha_{\text{o}}, 0)$ in the direction of the back polarizer at $\alpha_{\text{o}} = 45°$,

$$P^{\text{f}}_{\text{out}} = \frac{1}{2}\sqrt{\frac{\epsilon_0}{\mu_0}} \iint |\boldsymbol{\mathcal{E}}(x, y, L, t) \cdot \boldsymbol{n}|^2 \mathrm{d}x\, \mathrm{d}y\,. \tag{16}$$

We assume that the total power behind the polarizer is detected.

Backward light propagation starts with a 45° polarized Gaussian beam of equal shape and input power and ends with the projection (16) on a unit vector according to the front polarizer at $\alpha_{\text{i}} = 0$. With the backward output power $P^{\text{b}}_{\text{out}}$, isolation and transmission loss are defined as IS $= -10\log(P^{\text{b}}_{\text{out}}/P^{\text{f}}_{\text{out}})$ and LO $= -10\log(P^{\text{f}}_{\text{out}}/P_{\text{in}})$.

The significant refractive index contrasts of the materials under consideration cause these simulations to be somewhat questionable. Neither is the input Gaussian profile a valid electromagnetic field in the waveguide region, nor are the mode fields solutions of Maxwell's equations in the homogeneous region behind the waveguide end. With the simple overlap model, no realistic estimation of the power transition can be expected since the amounts of reflection, transmission, and radiation at input and output are not known with sufficient precision. A way out may be advanced modelling of the waveguide/air-transitions e.g. by means of more complex overlap integration [9] or least squares techniques [14] In this paper we do not tackle this problem. Besides, exact modelling of the rather artificial setup sketched above is not useful for a Faraday rotator in an integrated optics chip, e.g. in hybrid form [15].

However, at the two junctions the coefficients for reflection, transmission and radiation should be approximately equal for both directions of light propagation. Thus they cancel in the expression for the isolation, and we will obtain more realistic results.

Ideally in the backward direction the light that has passed the back polarizer should excite the modes of both polarizations with equal amplitudes. But at least in the case of the non embedded waveguides the profiles of TE- and TM-like modes differ slightly, and the initial amplitudes will be different as well, resulting in a small amplitude of the TE-like mode at the front polarizer. Additionally the hybrid TM-like mode has a small E_y component, and consequently at the front polarizer its contribution can not be completely suppressed.

4 Fabrication tolerances

An idealized treatment should be sufficient for estimating the fabrication tolerances. Assuming the final mode amplitudes of the forward analysis to be equal to the initial amplitudes of the backward simulation, the combined light paths are equivalent to a coupled mode propagation over twice the device length $2L$. In the forward direction no power is lost, $P_{\text{in}} = P^{\text{f}}_{\text{out}} = |C_{\text{TE}}(0)|^2$, while the power transmission in the backward direction is given by the final amplitude of the TE-like mode as $P^{\text{b}}_{\text{out}} = |C_{\text{TE}}(2L)|^2 = P^{\text{f}}_{\text{out}}(1 - \eta(2L))$, with TE and TM substituted for the mode indices in Eqs. (7, 9). Thus the deviation $\Delta\eta = 1 - \eta(2L)$ of the polarization conversion from unity becomes relevant. The effects mentioned at the end of the last section contribute another small fraction $rP^{\mathrm{f}}_{\mathrm{out}}$ of the power input to the backward output power, such that the total isolation is $\mathrm{IS} = -10\log(\Delta\eta + r)$.

Our model structures are formulated first in terms of parameters n_{s}, n_{f}, n_{c}, h, w, λ, which determine the wavenumbers and the shape of the basic modes. Then there are the quantities ξ and θ which are responsible for mode coupling and related to the length parameter L. Finally, perturbations like the diagonal anisotropy a must be checked. We will separately consider the influence of each of these parameters q, while all other quantities are kept fixed to their optimum values. If q is optimally adjusted as well, we have a phase matched waveguide of length $L_{\mathrm{c},q}/2$ with $\eta_q(L_{\mathrm{c},q}) = 1$. Changing q to $q + \delta q$ results in a lower conversion $\eta_{q+\delta q}(L_{\mathrm{c},q})$. The maximum deviation Δq for a given limited conversion degradation $\Delta\eta = 1 - \eta_{q+\Delta q}(L_{\mathrm{c},q})$ is defined as the tolerance of the parameter q.

4.1 Basic mode parameters

Assume q to be one of h, w, n_{s}, n_{c}, or n_{f} (where we keep ξ constant). In first order perturbation theory, a variation δq does not affect the shape of the basic mode fields and the coupling coefficient κ Eq. (5). At the same time, small propagation constant shifts $(\partial_q\beta'_j)\delta q$ detune the phase matching according to $\Delta\beta'_{q+\delta q} = (\partial_q\beta'_{\mathrm{TE}} - \partial_q\beta'_{\mathrm{TM}})\delta q$. Expanding $\eta_{q+\delta q}(L_{\mathrm{c},q})$ up to second order gives $\eta_{q+\delta q}(L_{\mathrm{c},q}) \approx 1 - (\partial_q\beta'_{\mathrm{TE}} - \partial_q\beta'_{\mathrm{TM}})^2\delta q^2/4|\kappa|^2$. For this quantity to be larger than $1 - \Delta\eta$, the parameter q may vary by no more than

$$\Delta q = \pm\frac{2|\kappa|\sqrt{\Delta\eta}}{|\partial_q\beta'_{\mathrm{TE}} - \partial_q\beta'_{\mathrm{TM}}|}\,. \qquad (17)$$

Obviously, along with κ, the tolerances for rib height, rib width and the refractive indices scale linearly with the off-diagonal permittivity ξ, i.e. linearly with the Faraday rotation Θ_{F}. Thus materials with improved magnetooptic effect will not only lead to shorter devices, but also to relaxed tolerance requirements.

For an evaluation of Eq. (17), expressions must be supplied for the gradients of the propagation constant. Regarding the refractive indices, one can directly use Eqs. (5) for the coefficients κ_{jj}, with a diagonal permittivity perturbation $2n_{\mathrm{s,f,c}}\Delta n_{\mathrm{s,f,c}}$ and with the integration extending over the substrate, core, and cover regions. Regarding the rib dimensions h and w, the continuity requirements of the electromagnetic fields at dielectric boundaries must be taken into account explicitely. Expressions for the variation of the propagation constant due to the shift of boundary locations have been investigated in [16]. According to those formulas, Δh and Δw are approximately inversely proportional to the relevant permittivity differences.

The coupling coefficient can be written as $|\kappa| = 2n_{\mathrm{f}}\Theta_{\mathrm{F}}R$ with a dimensionless factor R. Therefore, if we neglect in R the variation of the mode shape with respect to a wavelength alteration, κ remains fixed in first order, and Eq. (17) applies to the wavelength parameter λ as well. Observing that the propagation constants β are homogeneous functions of degree -1 in the relevant dimensional parameters, i.e. $\beta(x\lambda, xw, xh) = \beta(\lambda, w, h)/x$, their derivatives with respect to the wavelength can be expressed in terms of the h- and w-gradients:

$$\partial_\lambda\beta = -\frac{1}{\lambda}(\beta + w\partial_w\beta + h\partial_h\beta)\,. \qquad (18)$$

Note that Eqs. (17,18) applied to $q = \lambda$ assumes all material parameters to be fixed. A pronounced wavelength dependence of $n_{\mathrm{s,f,c}}$, Θ_{F}, or a must be taken into account by a combination of perturbation formulas or by explicit numerical evaluation.

4.2 Device length and magnetooptic parameters

The optimum length for a phase matched device is given by $L = \pi/4|\kappa|$. An alteration δL changes the power transfer ratio at the end of the relevant light path to $\eta(2(L + \delta L)) \approx 1 - (\pi\delta L/4L)^2$. Thus the tolerance for the device length is

$$\Delta L = \pm\frac{1}{2|\kappa|}\sqrt{\Delta\eta} = \pm\frac{1}{\pi}L_{\mathrm{c}}\sqrt{\Delta\eta}\,. \qquad (19)$$

ΔL is the only tolerance that turns out to be reciprocal to the Faraday rotation.

Regarding $\Theta_{\rm F}$ itself, expansion of $\eta_{\xi+\delta\xi}(L_{\rm c,\xi}) = \sin^2(\pi(1+\delta\xi/\xi)/2)$ leads to the tolerances

$$\Delta\xi = \pm\frac{2}{\pi}\xi\sqrt{\Delta\eta} \quad \text{or} \quad \Delta\Theta_{\rm F} = \pm\frac{2}{\pi}\Theta_{\rm F}\sqrt{\Delta\eta}. \tag{20}$$

Assuming the Faraday rotation to be the parameter with the most pronounced temperature dependence $\partial_T\Theta_{\rm F}$, an otherwise optimally tuned device should operate properly in a temperature range of

$$\Delta T = \pm\frac{2}{\pi}\frac{\Theta_{\rm F}}{\partial_T\Theta_{\rm F}}\sqrt{\Delta\eta}\,. \tag{21}$$

By evaluating $\eta_{\delta\theta}(L_{\rm c,0}) = \sin^2(\pi\cos(\delta\theta)/2)$, the magnetization angle θ can be shown to be the least critical quantity:

$$\Delta\theta = \pm\frac{2}{\sqrt{\pi}}(\Delta\eta)^{1/4}\,. \tag{22}$$

If one admits $\Delta\eta = 0.001$ (0.01), θ may deviate from the optimum $0°$ position by $\pm 11°$ ($\pm 20°$). While formally the nonreciprocal phase shift at an angle $\theta \neq 0$ must be considered as well, it turns out to be negligible when compared to the phase mismatch due to a detuned geometry (cf. the corresponding paragraph in Sec. 5.1).

4.3 Anisotropy

Changing the anisotropy parameter by δa shifts the propagation constants by $\delta a A_j/2$. Consequently, a must be known with a tolerance of

$$\Delta a = \pm\frac{4|\kappa|\sqrt{\Delta\eta}}{|A_{\rm TE} - A_{\rm TM}|}\,. \tag{23}$$

Compared to a device with isotropic core and dimensions w and h, a waveguide with anisotropic core achieves phase matching with slightly modified geometry, e.g. for parameters w and $h + \delta h$ with

$$\delta h = -\frac{a(A_{\rm TE} - A_{\rm TM})}{2(\partial_h\beta_{\rm TE} - \partial_h\beta_{\rm TM})}\,. \tag{24}$$

5 Numerical results

For this investigation mode fields and propagation constants for the isotropic, unperturbed structures were computed with the fully vectorial version of a recently proposed mode solver [17, 18]. It is based on local plane wave expansions for regions with constant permittivity. The semianalytical mode fields take the continuity requirements at dielectric interfaces explicitely into account and allow for a convenient evaluation of the various line- and surface integrals that arise from the perturbational theoretical treatment presented in the previous section.

Due to the extreme sensitivity of the phase matching condition this is one of the few occasions, where we have observed the semivectorial approximation [19] to be insufficient. With this approximation the shape of curves for the polarization conversion η (e.g. in Fig. 2(i)) remains, but the positions of the maxima are shifted by amounts exceeding the tolerances to be calculated. Therefore we used only fully vectorial, hybrid mode fields as a basis for the numerical experiments of the following section. Although our mode solver [18] is close to the state of art [20], the results for waveguide dimensions in Table 1 and the limit for the maximum achievable isolation should be looked upon with caution. However, the observed tendencies and estimates for fabrication tolerances seem to be reliable.

5.1 Raised strip waveguides

Device design starts with identifying suitable geometries where the fundamental modes are degenerate. For four arbitrarily chosen values of the waveguide width, the top left inset of Fig. 2 shows the rib height dependence of the fundamental effective mode indices. The curves for TE- and TM-like modes cross at a height h which is slightly smaller than the prescribed width w. Analogous curves can be drawn for the variation of the width for given rib height (top right inset).

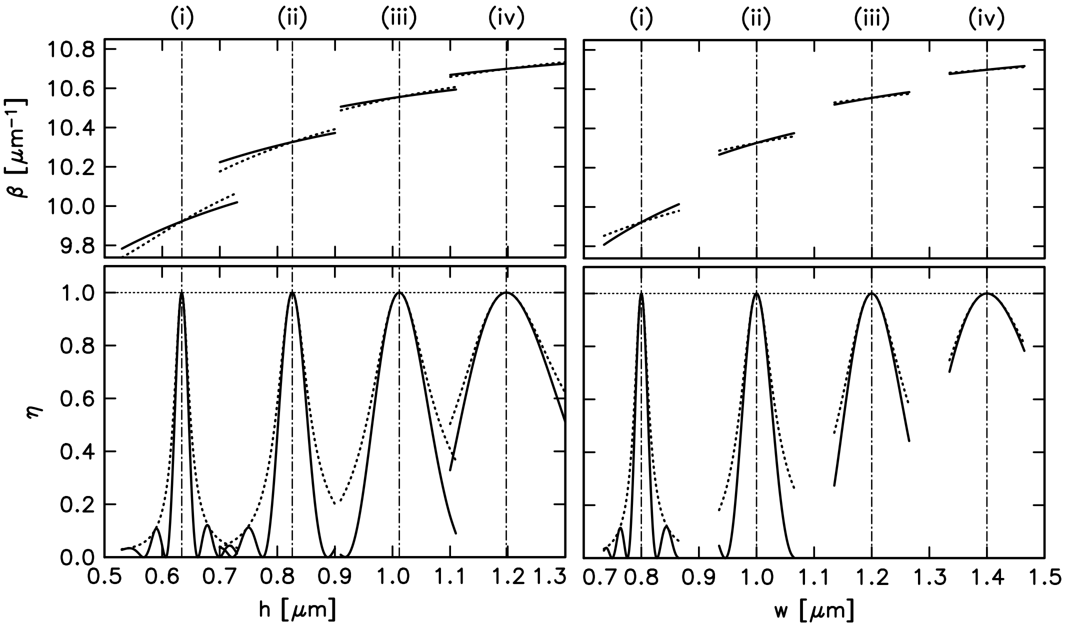

Figure 2: Propagation constants β (top) and polarization conversion η (bottom) versus the rib height h (left) and the rib width w (right) for waveguides as sketched in Fig. 1. For the four fixed values of the rib width (left) and rib height (right) see Table 1. In the top charts, continuous lines correspond to hybrid TE-like modes, dotted lines to modes with dominant TM polarization. Continuous lines in the bottom chart show the polarization conversion $\eta(L_c)$ at the fixed lengths L_c as given in Table 1, while the dotted lines indicate the maximum achievable conversion η_{max} at a length adjusted to the detuned height or width. The remaining parameters are the refractive indices $n_s = 1.95$, $n_f = 2.302$, $n_c = 1.0$, the nondiagonal permittivity element $\xi = 0.005$, anisotropy $a = 0$, and the vacuum wavelength $\lambda = 1.3\,\mu m$.

Table 1 summarizes the geometry data for the phase matched waveguides indicated by the crossing points. The tolerances for applications in an isolator setting can be evaluated by directly calculating the mode fields for a detuned geometry. Figs. 2 (bottom insets) and 3 show the dependences of the power transfer ratio η on rib height and width and wavelength variations. In the bottom parts of Table 1 these results are contrasted to perturbational values estimated with Eq. (17). There is good overall agreement, with the most pronounced differences occurring for the wavelength parameter λ. While the relevant derivatives $\partial_\lambda \beta_j$ can be accurately evaluated by Eq. 18 with a deviation below 1%, they are large (compared to $\partial_w \beta_j$, $\partial_h \beta_j$) and nearly equal. Therefore Eq. (17) with $q = \lambda$ gives the correct order of magnitude only, which should be sufficient since the wavelength turns out to be an uncritical parameter. Note that the limiting values for the polarization conversion $\Delta\eta$ can be translated into limits for the isolation IS $= -10\log(\Delta\eta)$ of 30 dB, 20 dB, 13 dB, 10 dB.

Regarding the parameters not listed in Table 1, we have observed the following tendencies. Influence of the cover refractive index is less significant. Due to the small field amplitudes at the rib/air-interface and to the low refractive index ($\delta\epsilon = 2n\delta n$) the tolerances Δn_c are roughly six times the values for the substrate refractive index.

If the magnetization offset-angle θ is regarded as a perturbational parameter, the polarization coupling is not affected in first order, while the TE/TM phase difference $\Delta\beta$ is slightly altered. This alteration turns out to be very small: for the four waveguides of Table 1, the nonreciprocal TM phase shift for a maximum angle of 10° can compensate the phase mismatch for a geometry deviation of about 1Å only. In the limit of a transversely adjusted magnetization the phase shift difference is equivalent to a geometry deviation still below 1 nm. Thus varying the direction of the magnetization cannot be used for tuning the phase matching (which can be achieved

	(i)		(ii)		(iii)		(iv)	
w/μm	0.8		1.0		1.2		1.4	
h/μm	0.6340		0.8260		1.0118		1.1975	
L_c/μm	357		325		315		309	
$\Delta\eta = 0.001$								
Δh/nm		*0.5*		*1.2*		*2.2*		*3.9*
Δw/nm		*0.4*		*1.0*		*2.1*		*3.8*
$\Delta\lambda$/nm	3	*2*	12	*4*	25	*10*	>40	*21*
$\Delta n_s/10^{-3}$		*1*		*2*		*4*		*7*
$\Delta n_f/10^{-3}$		*1*		*3*		*5*		*8*
$\Delta L/\mu$m		*4*		*3*		*3*		*3*
$\Delta\eta = 0.01$								
Δh/nm	1.5	*1.7*	3.2	*3.7*	6.3	*7.0*	11.2	*12.2*
Δw/nm	1.5	*1.4*	3.5	*3.3*	6.8	*6.6*	12.1	*11.9*
$\Delta\lambda$/nm	9	*6*	38	*16*	>40	*34*	>40	*66*
$\Delta n_s/10^{-3}$	4	*4*	9	*8*	16	*14*	25	*23*
$\Delta n_f/10^{-3}$	3	*4*	10	*8*	17	*15*	26	*26*
$\Delta L/\mu$m		*11*		*10*		*10*		*10*
$\Delta\eta = 0.05$								
Δh/nm	3.5	*3.9*	7.3	*8.3*	14.2	*15.7*	25.1	*27.3*
Δw/nm	3.4	*3.1*	7.9	*7.3*	15.3	*14.7*	27.1	*26.6*
$\Delta\lambda$/nm	19	*14*	>40	*35*	>40	*76*	>40	*149*
$\Delta n_s/10^{-3}$	8	*8*	21	*17*	36	*31*	56	*52*
$\Delta n_f/10^{-3}$	7	*8*	22	*18*	37	*34*	58	*58*
$\Delta L/\mu$m		*25*		*23*		*22*		*22*
$\Delta\eta = 0.1$								
Δh/nm	5.2	*5.4*	10.6	*11.7*	20.5	*22.2*	36.0	*38.6*
Δw/nm	5.0	*4.4*	11.3	*10.4*	22.1	*20.9*	38.7	*37.7*
$\Delta\lambda$/nm	>20	*20*	>40	*49*	>40	*108*	>40	*210*
$\Delta n_s/10^{-3}$	11	*11*	29	*24*	51	*44*	80	*74*
$\Delta n_f/10^{-3}$	11	*11*	31	*26*	52	*48*	80	*82*
$\Delta L/\mu$m		*36*		*33*		*32*		*31*

Table 1: Optimum dimensions h, w, conversion length $L_c = 2L$ and admissible fabrication tolerances for raised strip waveguides as sketched in Fig. 1 used as nonreciprocal polarization converters. Parameters not listed are as given for Fig. 2. Tolerances printed in italic style are determined by perturbation expressions, while the roman numbers have been read off from curves $\eta(q)$, with $q = h, w, \lambda, n_{f,s}$ as in Fig. 2, with the smaller difference taken in case of a nonsymmetric curve. See the text for a concise interpretation of the tolerances.

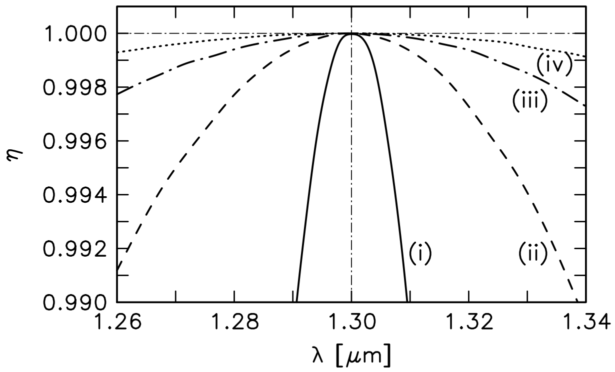

Figure 3: Polarization conversion η versus the operation wavelength λ for waveguides (i) to (iv) of Table 1. The degree of conversion η is evaluated at the fixed conversion lengths L_c corresponding to a wavelength of $\lambda = 1.3\,\mu$m. See Table 1 and the caption of Fig. 2 for parameters.

for one direction of propagation only, and is therefore less useful for isolator applications). On the other hand precise adjustment of this direction is less important. A larger deviation from the longitudinal direction will show up mainly in a conversion length alteration, where, for waveguides (i) to (iv), values $\Delta L_c = 2\Delta L$ below $6\,\mu$m ($20\,\mu$m) are tolerable. According to Fig. 4, θ must be adjusted to $\pm 11°$ ($\pm 20°$) to guarantee $\Delta\eta \leq 0.001$ ($\Delta\eta \leq 0.01$). The same result can be obtained with the perturbational formula (22).

For $\Delta\eta$ below 0.001 (0.01), the nondiagonal permittivity element must be kept at $\xi = 0.005$ with tolerances of $\pm 1.0 \cdot 10^{-4}$ ($\pm 3.2 \cdot 10^{-4}$). This corresponds to tolerances for the Faraday-rotation $\Theta_F = 3000°/\text{cm}$ of

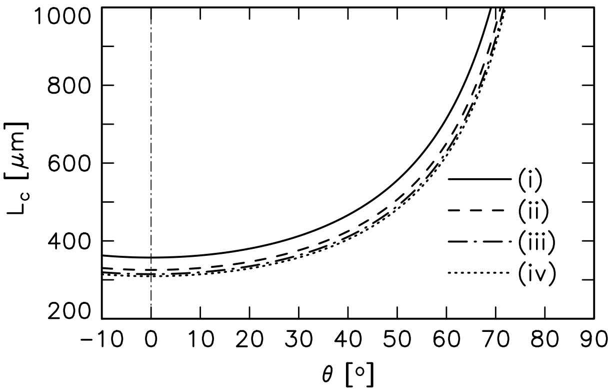

Figure 4: Conversion length L_c versus the angle θ of the magnetization with respect to the longitudinal direction, for the four waveguides of Table 1.

$\pm 60°/\mathrm{cm}$ ($\pm 191°/\mathrm{cm}$). For a typical temperature coefficient $\partial\Theta_\mathrm{F}/\partial T = 3.19°/\mathrm{cmK}$ at room temperature [21], the temperature should deviate by no more than 19 K (60 K), if the temperature coefficients of all other material parameters are neglected.

In contrast to the phase shifts induced by refractive index changes, the shifts (13) due to a variation of the anisotropy parameter a have different signs for the modes of different dominant polarizations. Thus a must be known with accuracy one order of magnitude higher. According to Eq. (23), $\Delta a/10^{-4}$ evaluates to 3, 10, 22, 31, for given $\Delta\eta$ of 0.001, 0.01, 0.05, 0.1, and uniformly for waveguides (i) - (iv). To compensate for anisotropy, the basic geometry must be significantly changed. From Eq. (24), we obtain values for $(\delta h/a)/\mu$m of 1.8, 3.8, 7.1, and 12.3 for waveguides (i) to (iv). For an anisotropy $a = 0.01$, the rib height of device (iv) should deviate by 123 nm from the value given in Table 1 to restore phase matching. In this case consideration of anisotropy is indispensable.

Figs. 5, 6 illustrate the relevant components of the normalized fundamental modes in waveguides (i) and (iv). The E_x-components of TM-like solutions appear almost equal in magnitude and shape to the E_y-components of the TE-like modes, with only small deviations, caused by dielectric discontinuities. There the field strength and thus the absolute difference is more pronounced for the small core of waveguide (i). As can be seen by inspecting Eqs. (5, 17), this results in larger differences of the wavenumber derivatives, and thus in the tight tolerances, of (i) compared to (iv).

According to Fig. 5 even for device (i) almost all of the mode power is concentrated in the core region. Thus by Eq. (15) the attenuation constants α_j/D evaluate to a value close to unity, with differences of about 5% (i) and 1% (iv) between TE- and TM-like modes. With typical values for D as low as 1 cm^{-1} [22], for waveguides (i) to (iv) the relevant quantity $(\alpha_\mathrm{TE} - \alpha_\mathrm{TM})/4|\kappa|$ remains below 10^{-4}. Attenuation of both fundamental modes is almost equal and will not deteriorate the isolation.

Due to the similar mode profiles, an initial field that has passed a polarizer at an angle of 45° excites both modes with identical amplitudes. For backward propagation, the amplitude ratio $|C_\mathrm{TE}/C_\mathrm{TM}|^2$ is indeed below 10^{-5} in the numerical simulations of setups for waveguides (i) to (iv).

Nevertheless, we obtained numerical upper limits for the isolation of about 25 dB, 30 dB, 32 dB, and 35 dB for these devices. These bounds are due to the hybrid nature of the modes. In the backward direction at the position of the front TE-adjusted polarizer, almost all of the inserted power is carried by the TM mode. In our model, the polarizer blocks its large E_x-part, but the power in the small E_y component passes. As it should be, the ratios $\iint |E_y|^2 \mathrm{d}x\,\mathrm{d}y / \iint |E_x|^2 \mathrm{d}x\,\mathrm{d}y$ for the TM modes of the four waveguides evaluate to the above given numbers for the maximum isolation. Note, that these values depend crucially on the model for the waveguide-air transition. For the TE modes we have observed ratios of the powers assigned to x- and y-components that are almost reciprocal to the ratios given above, thus changing to TM input will not enlarge the peak isolation.

(i) and (ii) are single mode waveguides. For (iii) and (iv), both rib height and width are enlarged, thus they support a total of six modes, one additional mode with a horizontal and one with a vertical nodal line for each polarization. Due to their asymmetric shape and differences of propagation constants, coupling with the fundamental modes will not occur. If higher order modes are excited, about half of the power passes the device in both directions and degrades the isolation. However, by means of properly focused input beams it should be possible to suppress this phenomenon. With circular Gaussian fields adjusted to the fundamental mode shape,

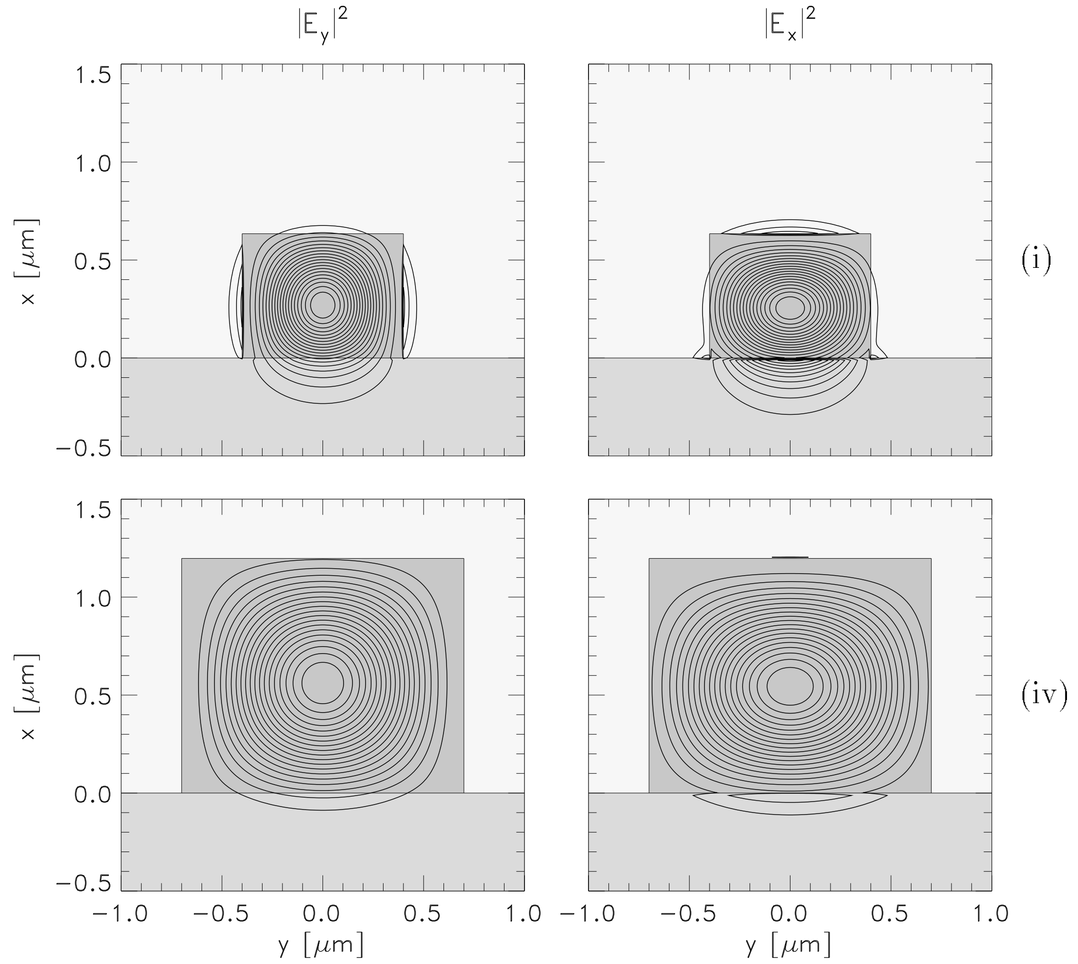

Figure 5: Mode intensity profiles for the dominant field components of the fundamental modes for waveguides (i) (top) and (iv) (bottom) in Table 1. The contours show the squared E_y-components of symmetric, TE-like modes (left) and the squared E_x-component of the antisymmetric, TM-like modes (right).

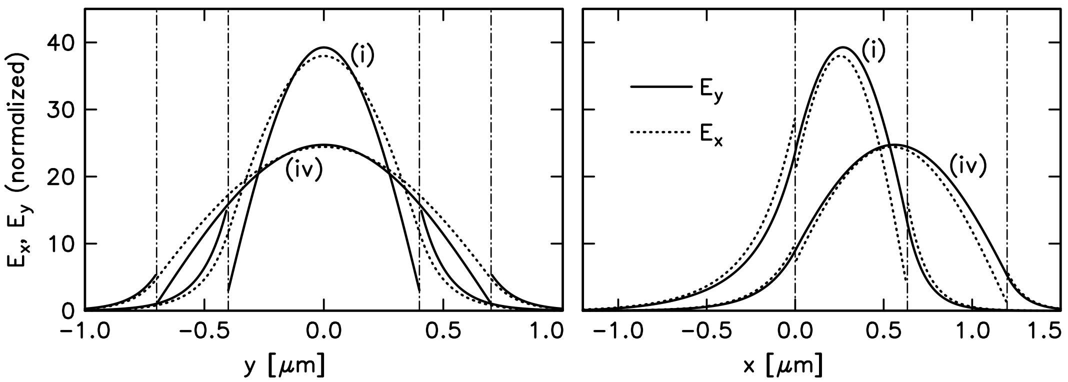

Figure 6: Profile sections of the dominant field components of the fundamental modes for waveguides (i) and (iv) in Table 1. Continuous lines correspond to E_y-components of symmetric, TE-like modes, dotted lines to the E_x-component of the fundamental antisymmetric, TM-like modes. For the left chart, fields have been evaluated on horizontal lines at $x = 0.26\,\mu$m (i) and $x = 0.55\,\mu$m (iv), close to the amplitude maxima. The right chart shows the mode amplitudes along the waveguide symmetry plane at $y = 0$.

the power fraction assigned to higher order modes could be kept well below 10^{-3} in our simulations.

If a polarization rotating waveguide is to be used in an integrated isolator device, e.g. in a hybrid setup [15], the relative adjustment of the components will be important. The effects of the two polarizer angles are easily accessible from our model. Fig. 7 shows their influence on the isolation. For an isolation larger than 20 dB, both polarizers may not deviate by more than $\pm 5^\circ$ from the optimum 0° and 45° positions, respectively. Both charts show the maximum levels of the isolation. Due to the small difference between the shapes of TE and TM modes, the locations of the maxima are slightly shifted from the 0° and 45° positions. Obviously this effect can well be neglected even for strongly guiding cores.

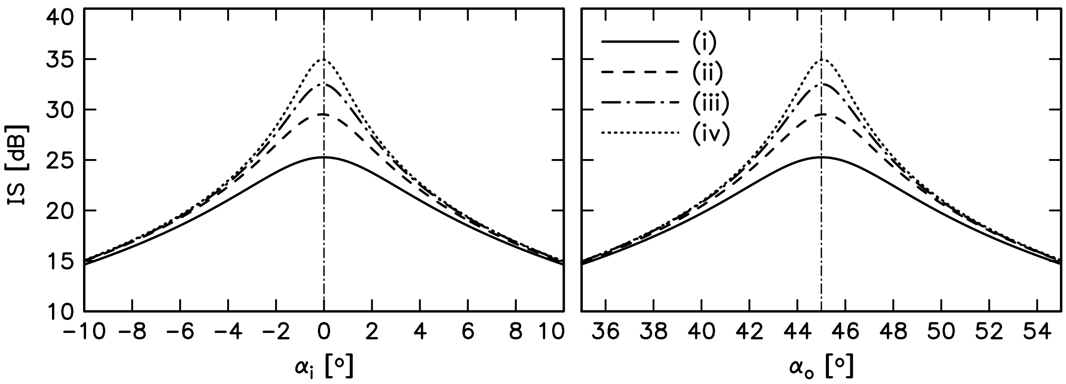

Figure 7: Isolation IS versus the angles α_i, α_o, of the polarizers at input (left) and (output) of an isolator setting employing the Faraday rotating waveguides of Table 1. An angle of 0° corresponds to linear polarization in the y-direction.

5.2 Embedded waveguides

For embedded waveguides surrounded by a homogeneous cladding the phase matching condition is realized if, apart from the magnetooptic effect, the core material is isotropic. Fig. 8 summarizes results for a series of such waveguides with varying core dimension and for parameters as in Sec. 5.1.

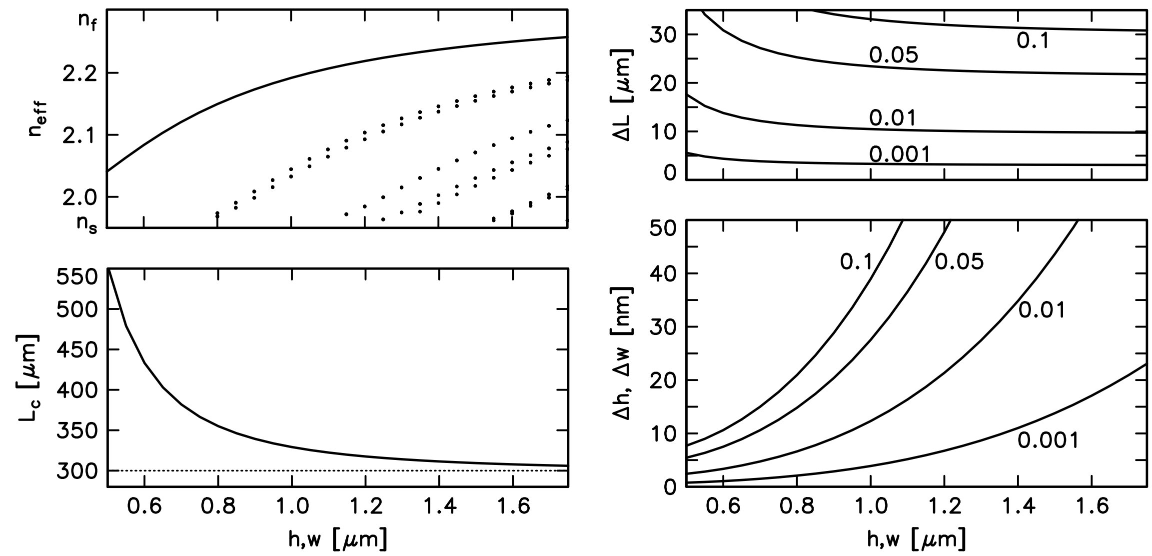

Figure 8: Effective mode indices n_eff, conversion length L_c (left) and geometry tolerances Δh, Δw, ΔL (right) versus the height and width h, w of the core for embedded waveguides of square shape. Parameters are $n_s = n_c = 1.95$, $n_f = 2.302$, $\xi = 0.005$, $\lambda = 1.3\,\mu$m (see Fig. 1). The allowed polarization conversion deviation $\Delta\eta$ is the curve parameter in the charts on the right.

According to Fig. 8, up to a width of about $0.8\,\mu$m the waveguides support only one mode for each polarization. For larger cores higher modes appear, all are twofold degenerate. The closely spaced dotted lines correspond to four first order modes with one nodal line in the dominant electric component, in a direction parallel or perpendicular to the polarization. Therefore they are not fourfold degenerate.

For smaller cores less power is guided inside the magnetooptic region. Thus the mode coupling weakens, the conversion length L_c increases. The bigger cores convert the polarization along a distance already close to the length $L_c^{\mathrm{bulk}} = 300\,\mu$m for plane waves in a magnetooptic bulk medium.

Since we have kept constant the value of the Faraday-rotation, the conversion length tolerances ΔL_c are also similar to the results for the uncovered strips. At the same time, the lower permittivity contrast relaxes the tolerance requirements Δh, Δw significantly. Core height and width alterations have equal effects. Scaling the waveguide does have little influence on the polarization conversion, deviation of the core shape from a square matters. The tolerances give the maximum allowed absolute difference between the core width and height.

Due to the symmetry of the problem, in the lowest relevant order the dependence of the polarization conversion on refractive index and wavelength variations vanishes. Thus these tolerances are much larger than those worked out in Sec. 5.1.

For the embedded waveguides one can again evaluate the isolation limits caused by the small mode components. As shown in Fig. 9, these values do not deviate much from those for the raised strip waveguides of comparable height and width.

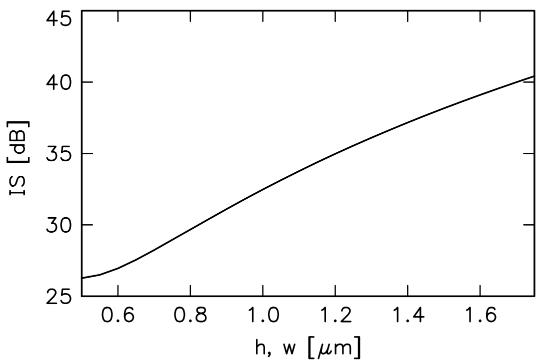

Figure 9: Limit for the achievable isolation IS for square embedded magnetooptic wavguides versus height and width h, w of the core. Parameters are as in Fig. 8.

6 Conclusions

Phase matching as a condition for complete polarization rotation can be realized with selected geometries of raised strip waveguides or embedded square waveguides. In the framework of coupled mode theory for magnetooptic cores we have considered linear birefringence and absorption as well as the influence of geometry and wavelength variations via simple and efficiently implementable perturbational expressions. Agreement with directly calculated values is sufficient for the purposes of tolerance estimation in an isolator setting.

The accuracy requirements for embedded waveguides are less critical than for simple raised strips. At the same time, manufacturing will be more involved, and the waveguides are not accessible for additional tuning steps.

Unfortunately, most tolerances turn out to be very strict. Ab initio fabrication of a waveguide with 30 dB isolation in a conventional experimental setup is difficult. Postfabrication tuning, such as suitable annealing or etching the rib surface, will be necessary. Alternatively, proper performance can be achieved simply by lining up more than one isolating section. This requires input and output polarization to be equal, thus optical active waveguide sections must be added. Then substituting the polarizers by polarization splitters results in an all integrated optical device, where input and output channels are guided modes. In that case problems like the limited isolation due to hybrid mode fields or reflections and losses at the waveguide-air interfaces do not occur.

Acknowledgment

Financial support by Deutsche Forschungsgemeinschaft (Sonderforschungsbereich 225) is gratefully acknowledged.

References

[1] P. K. Tien, R. J. Martin, R. Wolfe, R. C. Le Craw, and S. L. Blank. Switching and modulation of light in magneto-optic waveguides of garnet films. *Applied Physics Letters*, 21:394–396, 1972.

[2] J. Warner. Nonreciprocal magnetooptic waveguides. *IEEE Transactions on Microwave Theory and Techniques*, MTT-23:70–78, 1975.

[3] M. Monerie, A. Leclert, P. Anizan, G. Moisan, and P. Auvray. Dispositifs magnetooptiques en couches minces a accord de phase: utilisation d'une double heteroepitaxie de grenats ferromagnetiques. *Optics Communications*, 19:143–146, 1976.

[4] K. Ando, N. Takeda, N. Koshizuka, and T. Okuda. Annealing effects on growth induced optical birefringence in liquid-phase-epitaxial-grown Bi-substituted iron garnet films. *Journal of Applied Physics*, 57:1277–1281, 1985.

[5] H. Dammann, E. Pross, G. Rabe, W. Tolksdorf, and M. Zinke. Phase matching in symmetrical single-mode magneto-optic waveguides by application of stress. *Applied Physics Letters*, 49:1755–1757, 1986.

[6] H. Dammann, E. Pross, G. Rabe, and W. Tolksdorf. 45° waveguide isolators with phase mismatch. *Applied Physics Letters*, 56:1302–1304, 1990.

[7] R. Wolfe, V. J. Fratello, and M. McGlashan-Powell. Thin-film garnet materials with zero linear birefringence for magneto-optic waveguide devices. *Journal of Applied Physics*, 63(8):3099–3103, 1988.

[8] R. Wolfe, R. A. Lieberman, V. J. Fratello, R. E. Scotti, and N. Kopylov. Etch-tuned ridged waveguide magneto-optic isolator. *Applied Physics Letters*, 56(5):426–428, 1990.

[9] C. Vassallo. *Optical Waveguide Concepts*. Elsevier, Amsterdam, 1991.

[10] S. Yamamoto and T. Makimoto. Circuit theory for a class of anisotropic and gyrotropic thin-film optical waveguides and design of non-reciprocal devices for integrated optics. *Journal of Applied Physics*, 45:882, 1974.

[11] M. Shamonin and P. Hertel. Analysis of nonreciprocal phase shifters for integrated optics by the Galerkin method. *Optical Engineering*, 34(3):849–852, 1995.

[12] A. F. Popkov, M. Fehndrich, M. Lohmeyer, and H. Dötsch. Nonreciprocal TE-mode phase shift by domain walls in magnetooptic rib waveguides. *Applied Physics Letters*, 72(20):2508–2510, 1998.

[13] R. Gerhardt, S. Sure, H. Dötsch, T. Linkewitz, and W. Tolksdorf. Optical properties of bismuth and gallium substituted thulium iron garnet films. *Optics Communications*, 102:31–35, 1993.

[14] B. M. A. Rahman and J. B. Davies. Analysis of Optical Waveguide Discontinuities. *Journal of Lightwave Technology*, 6(1):52–57, 1988.

[15] N. Sugimoto, H. Terui, A. Tate, Y. Katoh, Y. Yamada, A. Sugita, A. Shibukawa, and Y. Inoue. A Hybrid Iintegrated Waveguide Isolator on a Silica-Based Planar Lightwave Circuit. *Journal of Lightwave Technology*, 14(11):2537–2546, 1996.

[16] M. Lohmeyer, N. Bahlmann, and P. Hertel. Geometry tolerance estimation for rectangular dielectric waveguide devices by means of perturbation theory. *Optical and Quantum Electronics*, 1998. submitted.

[17] M. Lohmeyer. Wave-matching method for mode analysis of dielectric waveguides. *Optical and Quantum Electronics*, 29:907–922, 1997.

[18] M. Lohmeyer. Vectorial wave-matching mode analysis of integrated optical waveguides. *Optical and Quantum Electronics*, 1998. accepted for publication.

[19] M. S. Stern. Semivectorial polarised finite difference method for optical waveguides with arbitrary index profiles. *IEE Proceedings, Pt. J*, 135(1):56–63, 1988.

[20] C. Vassallo. 1993-1995 Optical mode solvers. *Optical and Quantum Electronics*, 29:95–114, 1997.

[21] M. Wallenhorst, N. Bahlmann, V. Backherms, A. Josef, P. Hertel, and H. Dötsch. Optimized nonreciprocal rib waveguides for integrated magneto-optic isolators. In K. Rubin, J. A. Bain, T. Nolan, D. Bogy, B. J. H. Stadler, M. Levy, J. P. Lorenzo, M. Mansuripur, Y. Okamura, and R. Wolfe, editors, *High-Density Magnetic Recording and Integrated Magneto-Optics: Materials and Devices*, MRS Spring Meeting Proceedings, San Francisco, 1998, to appear.

[22] H. Dötsch, P. Hertel, B. Lührmann, S. Sure, H. P. Winkler, and M. Ye. Applications of Magnetic Garnet Films in Integrated Optics. *IEEE Transactions on Magnetics*, 28(5):2979–2984, 1992.